Received: 3 August 2017 | Revised: 2 April 2018 | Accepted: 21 April 2018

DOI: 10.1002/we.2208

RESEARCH ARTICLE

WILEY

Comparison of nondestructive testing techniques for the inspection of wind turbine blades' spar caps

Robert W. Martin[1] | Alessandro Sabato[2] | Andrew Schoenberg[3] | Robert H. Giles[1] | Christopher Niezrecki[2]

[1] Physics Department, University of Massachusetts Lowell, 1 University Avenue, Lowell 01854MA, USA

[2] Department of Mechanical Engineering, University of Massachusetts Lowell, 1 University Avenue, Lowell 01854MA, USA

[3] Composites Engineering Research Laboratory, TechPlace, 74 Orion Street, Brunswick 04011ME, USA

Correspondence
Robert W. Martin, Physics Department, University of Massachusetts Lowell, 1 University Avenue, Lowell, 01854 MA, USA.
Email: robert_martin1@student.uml.edu

Funding information
National Science Foundation, Grant/Award Number: IIP-1362022

Abstract

To increase the energy conversion efficiency and power production, the size of wind turbine blades has continued to grow larger. As such, the need to identify defects and monitor the structural health becomes more critical to maintain reliability and prevent costly catastrophic failures. Larger blades are subject to an increased likelihood of operational damage and manufacturing defects. Usually, glass-reinforced spar caps are inspected with the assistance of strong flashlights, while nondestructive testing (NDT) inspections are performed only on carbon-reinforced blades which are not translucent. These operations provide qualitative information only. Therefore, there is a growing need for inspection techniques that can provide quantitative information for assessing the structural health of the blades. In recent years, different NDT techniques capable of accurately delivering surface and internal data have been developed. Nondestructive testing systems should be able to quickly and efficiently scan large areas, to be economically beneficial to the wind turbine manufacturing industry. Within this paper, 3 different NDT techniques for the inspection of manufactured wind turbine blades' spar caps are compared: terahertz inverse synthetic aperture radar, infrared thermography, and X-ray imaging. Each is investigated to evaluate their ability to detect the presence of defects of concern that are created during the blade manufacturing process. Through a set of experimental tests, the advantages, challenges, and drawbacks of each used technique are evaluated and compared in the context of the needs of the wind turbine industry. This research provides the foundation of empirical comparisons that can lead to the development of more accurate NDT resulting in the construction of more reliable and less-expensive wind turbine blades.

KEYWORDS

infrared thermography, nondestructive testing, terahertz inverse synthetic aperture radar, wind turbine blades, X-ray imaging

1 | INTRODUCTION

Wind energy continues to grow as a significant source of renewable energy in the world's energy sector. Statistics and forecasts released by the Global Wind Energy Council (GWEC) in 2015 showed that the expected global cumulative installed wind capacity would grow to 25% in the next 5 years. It will reach the threshold of 800 GW by 2020.[1] Turbine makers are developing systems able to produce up to 20 MW per turbine, which means having a rotor blade diameter more than 100 m.[2] Therefore, as the size of wind turbines (WTs) increases, ensuring the structural integrity of

 Copyright © 2018 John Wiley & Sons, Ltd.

its components becomes essential. This is even more evident if it is assumed that the 20-year life operations and maintenance (O&M) costs for a single WT might account for about 75% to 90% of the turbine capital investment.[3]

The blades of a WT play a key role, as they are the elements used for converting the atmospheric wind energy to mechanical kinetic energy. An ideal blade should incorporate progressive variations in twist, planform, chord, thickness, and aeroelastic properties to take into account the differences in the airspeed between its tip and root.[4] As a result, blades have an airfoil cross section similar to that shown in Figure 1 where components such as leading edge, trailing edge, spar cap, shear webs, and sandwich panels are highlighted.

Because of the high bending stiffness required to bear with the static and dynamic loads experienced by an in-service blade, a fiberglass laminate, carbon fiber-reinforced plastic (CFRP), and fiberglass construction with the selective use of carbon for local reinforcement are the current materials of choice for WT blade manufacturing.[5] For instance, carbon fibers or pultruded glass fibers are used for some specific structural areas of the blades such as the spar cap to allow for better resistance to the flap-wise bending loads.[6] However, owing to the lower cost and acceptable structural properties, fiberglass is the most extensively used material.[7] Finally, blade skins, typically made from double bias or triaxial fiberglass fabrics with a balsa or foam core, are used to increase thickness and improve buckling resistance.[6] The different components of the blade are manufactured and assembled by a pressure resin infusion technique like the vacuum-assisted resin transfer molding (VARTM) or by preimpregnated technology in open or closed molds, where the fibers are usually laid manually.[7,8]

Wind turbines can experience diverse kinds of failure at different locations of the structure. A 15-year survey made with a population of nearly 35 000 WT showed that the most likely components to fail are electrical systems (23%), plant control systems (18%), sensors (10%), yaw systems (8%), rotor blades (7%), and mechanical brakes (6%).[9] Although blade failures are reported as the fifth most common cause of failure, owing to their exposure to extreme environments, tips and blades experience the first and third failure rate compared to the other structural components. In particular, a study conducted on the reliability of WTs highlighted a failure rate of 1.00×10^{-4} failures per hour and 1.12×10^{-5} failures per hour for tips and blades respectively.[10] Review of primary data sources indicated that between January 1996 and September 2017, 2159 WT damage incidents had occurred worldwide. Events classified as "blade failure" comprised 17.4% (375) of the total.[11] In 2015, WT blades failed at a rate of nearly 3800 failures per year (ie, 0.54% of the almost 700 000 blades operated worldwide).[12] Analyses performed on collapsed WTs found that insufficient strength and poor quality control of materials were the causes of the blades' collapse during high winds.[13,14] These data highlight the need to ensure the quality of produced blades and certify that the whole population of a blade type fulfills the design assumptions to an acceptable level of probability.

The level of automation in the modern WT blade manufacturing process varies by manufacturer, and as blades increase in size, the probability and the number of manufacturing defects increase. As large blades are produced, the stronger and less-expensive reinforcing fabrics are desired and preimpregnated plies may be used to achieve improve manufacturing efficiency. Increases in fabric weight may create problems associated with ply drops where the thickness is tapered.[15] There are a variety of ways in which a blade can be damaged, both in the field and during the manufacturing process. Damage characteristics of the manufacturing process include defects like delamination, waviness, inclusions, voids, cracks, resin dry regions, and improper fiber alignment. All of the above can potentially cause blade failure long before the expected end of design life.[16,17] These defects may be because of mistakes in the deployment of the fabric during the manufacturing process (eg, fabric joints and overlaps where individual rolls of plies terminate). Delamination between plies produces cracks that propagate through the laminate.[18] While this type of defect can sometimes be linked to a number of potential causes, it is usually driven by a tensile or compressional load (ie, buckling) that produces an internal damage that grows till it reaches the interface between face and core in the sandwich panels.[19] Often in composites, delamination is accompanied by the formation of a crack bridging zone, where intact fibers connect the crack faces behind the crack tip.[20] Delamination of laminates and adhesively bonded joints are usually the most critical failure as they induce a reduction of blade stiffness that can propagate through the whole structure causing sudden failure.[21] A comprehensive description of this failure mechanism can be found in the literature.[22] In-plane waviness is a significant flaw that can occur during the manufacturing process. It can be seen that geometrical distortions of the plies result in a considerable decrease of mechanical integrity of the localized region.[23] Strength is reduced because of 2 factors: The fibers are already in a buckled configuration (ie, a significant mode of compressive failure), and they are not aligned or disoriented.[24] Inclusion defects are generated by the presence of foreign bodies within the composite layers.[25] Voids are caused by air bubbles trapped in the laminate during the curing cycle or by nucleation from volatiles during processing.[26] Dry spots are areas of poor or no bonding between adjacent plies caused by trapped air or a weak infusion of resin in the given area. This kind of defect can cause the debonding of the 2 interfaces that it affects, and it can be triggered by buckling-driven loads. Figure 2 provides a sketch illustrating common manufacturing defects on a WT blade.

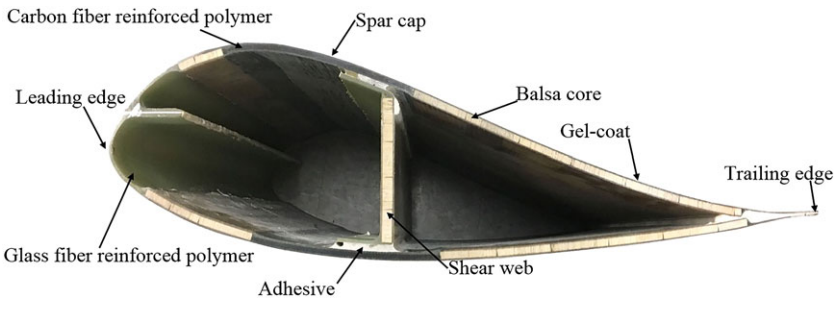

FIGURE 1 Cross section of a typical WT blade near the tip with subcomponents and materials highlighted [Colour figure can be viewed at wileyonlinelibrary.com]

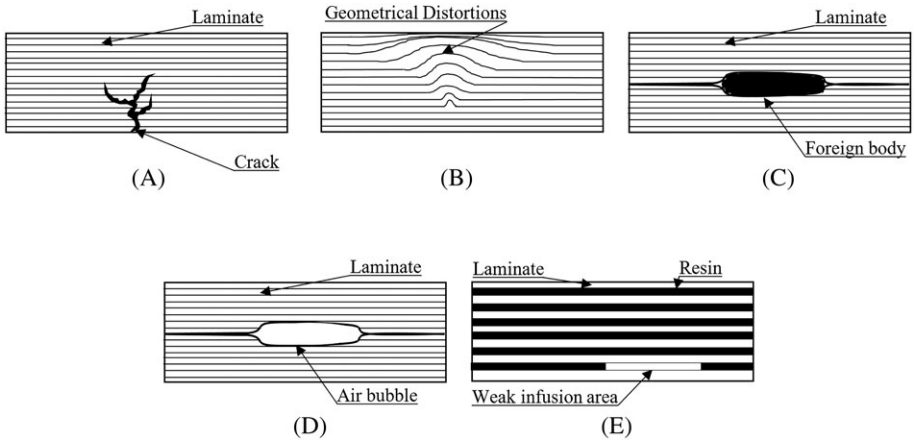

FIGURE 2 Illustration of the common manufacturing flaws in a WT blade. A, Delamination and cracks. B, Out-of-plane waves. C, inclusions. D, Voids. E, Resin dry regions

While design flaws can be engineered to reduce the likelihood of failure, manufacturing flaws may occur at random concerning type, size, and location. Manufacturing defects such as those listed often cannot be detected using visual inspection, creating a growing need for nondestructive testing (NDT) techniques that are capable of scanning the blades over large areas to identify the presence or absence of these flaws. This work studies the effectiveness of 3 techniques at producing contrast between regions with and without defects. The 3 techniques are terahertz inverse synthetic aperture radar (ISAR), infrared thermography (IRT), and X-ray imaging. Each of these methods was tested using 3 fiberglass samples designed explicitly for this evaluation. These specimens contain intentionally embedded imperfections (ie, delamination, wave defects, dry resin areas, and inclusions) that are representative of the manufacturing defects that are of concern for composite and wind turbine manufacturing companies. The paper is organized as follows: Section 2 presents an overview of the operational principles of the selected NDT techniques. In Section 3, a detailed description of the composite fiberglass panels and the embedded defects is provided. The results of the laboratory experiments performed for evaluating the performance of different NDT techniques are discussed in Section 4. Finally, conclusions are drawn, and future work is briefly outlined in Section 5. It should be noted that this is not the first time some of these techniques have been compared together.[27] Nevertheless, it is the first attempt to use the terahertz ISAR methods for performing NDT evaluations of WT blades, and it is the first attempt to compare those results with X-ray and IRT inspection for a systematic set of test samples having a variety of defects representative of the real-world WT composites manufacturing process.

2 | BACKGROUND

Conditioning monitoring (CM), structural health monitoring (SHM), and NDT all play a fundamental role in assessing the condition of WT blades and preventing catastrophic failures. CM and SHM techniques (eg, acoustic emission, fiber optic methods, modal parameters estimation, process parameters, shock pulse methods, and strain measurements) are used to assess the ongoing performance of the component while it is in operation. However, NDT is typically used during or postmanufacturing to confirm that the manufacturing conforms to specifications or it is commonly used to monitor the structures before, during, and after deployment. In this paper, emphasis is given to NDT techniques only, leaving the discussion about CM and SHM to the specialized literature.[28-31]

Several NDT systems have been proposed over time for assessing the conditions of WT blades, and each possesses their advantages and challenges. Ultrasonic waves have been well investigated in NDT.[28] The fundamental principle of the technique is that an ultrasonic wave is either passed through the material or is reflected, resulting in an identifiable signal that is directly related to a defect. The method may be applied both to a single transmitter/receiver transducer (ie, pulse-echo mode) and with separate transmitter and receiver transducers placed on the same or opposite sides of the material.[32] Although this technique can efficiently identify defects in relatively thick laminates, ultrasonic systems interrogate only a small footprint (a few square centimeters) and are currently too slow to scan the entire surface areas of the blades. Therefore, current postmanufacturing inspections are limited to only the most critical areas of concern.

Another method used for scanning the internal part of the composite material involves eddy current. By inducing electrical currents in the material being tested, and recording the variation of the induced currents, it is possible to inspect conductive materials.[33] Variations in the structure of the specimen examined will cause a change in the current flow highlighting the presence of defects. A similar method is the electrical resistance-based damage detection method, which relies on the conductive property of the CFRP. By using 2 electrodes placed outside the plies, it is possible to detect the electrical resistance change in the CFRP composite laminate as a defect is introduced into the layers between the electrodes.[34] Nevertheless, their application is limited to CFRP components only having conductive/magnetic characteristics. Another class of NDT techniques that have drawn interest from the industry is optical NDT techniques. Laser speckle interferometry uses the intensity distribution pattern generated by illumination of coherent light onto rough object surfaces for detecting deformation profiles over the surface of the structure

indicative of internal defects.[35] What should also be noted is that laser speckle interferometry has been recently combined with digital image correlation (DIC) for providing full-field measurements of geometry and strain profile of the blade.[36,37] As a downside, these 2 approaches are surface inspection techniques and therefore only provide limited information about the defects embedded inside the plies.

Other techniques have been used to detect abnormalities embedded underneath the surface of the plies. One of the most common is IRT, a technique that relies on the detection of the temperature field emitted by a body having a temperature *T*. It is used in a variety of fields including medicine,[38] agriculture,[39] environmental monitoring (eg, pollution detection in rivers and the sea,[40] indoor climate),[41] maintenance (eg, mechanical equipment,[42] building diagnostics),[43,44] and nondestructive evaluations (eg, defects and anomalies detection in various civil engineering structures).[45-47] This technique relies on the thermal energy emitted by a body, which is a function of its external temperature and emissivity (ie, its effectiveness in emitting power as thermal radiation). It allows plotting a thermal map of the object being tested based on the temperature measured by the camera's sensing elements associated with each pixel. Of primary interest in this paper are applications of IRT to the inspection of composites. In general, IRT describes a broad set of inspection techniques, many of which have been extensively investigated as NDT techniques for fiberglass composites. Active and passive infrared thermography of various forms has been used to image, detect, and evaluate multiple fiberglass composite materials.[48] Similar methods have also been used to observe the time evolution of fatigue-based defects over time as well as to inspect rotor blades with laboratory and field test evaluation.[49] Although the specific benefits of thermography vary by technique, IRT, in general, brings several advantages including higher inspection speed, higher resolution and sensitivity, improved detection of subsurface defects, and the methods, in general, do not require a couplant.

Other IRT approaches available depends on the specific solicitation input to the system (ie, flash thermography, pulsed thermography, modulated thermography, pulse-phase thermography, ultrasonic lock-in thermography). Pulsed thermography involves briefly heating the specimen and then recording its temperature decay curve. Because of its characteristics in highlighting differences in the material thermal properties, this technique has been used for detecting adhesive defects of glass fiber-reinforced plastic (GFRP) composite plates.[50] In the modulated thermography, the specimen is exposed to a sinusoidal temperature stimulation. The modulated frequency of the thermal stimulation can be tuned depending on the specific case, providing this technique with improved depth resolution. Pulse-phase thermography combines advantages both of pulse (PT) and modulated infrared thermography simultaneously. The specimen is pulse heated as in PT, and the mix of frequencies of the thermal waves introduced into the test object are deconvolved by performing the Fourier transform of the temperature evolution over the field of view.[51] The pulsed-phased method has been used for detecting the cellular structure of honeycomb structures and assessing the condition of a portion of a wind turbine blade. In 1 study, the proposed system was able to detect defects having increasing severity (ie, diameter) as deeper layers were[52], while in another study, a panel characterized by initially prepared flaws and improper resin impregnation was studied.[53] Because of its accuracy in detecting subsurface flaws, thermography continues to grow in popularity as an NDT technique in the composite materials industry. Several research efforts have proven the capability of this class of techniques to detect delamination defects with accuracy comparable to other commonly used techniques.[54] Both active and passive approaches using thermography has been shown to be capable of detecting defects such as the formation of strain patterns anticipating cracks during fatigue tests,[55] as well as adhesive defects, delamination, and mechanical loading.[56]

Radar-based techniques using millimeter-wave and terahertz technology radiation have been successfully proposed as NDT methods.[57] Radar transmission measurements using frequency bands of ~24 GHz showed a high penetration depth in glass fiber-reinforced materials and the possibility to detect water pockets inside the rotor blade.[58] Terahertz waves were explored as an NDT tool for identifying and characterizing flaws and damage in nonconducting composites and conducting composites using both time-domain spectroscopy and continuous wave approaches.[59-66] Terahertz techniques were used for detecting delamination defects in panels simulating the WT blade structure, proving the capability to highlight flaws as thick as 1×10^{-3} m. Furthermore, previous investigations into the use of terahertz synthetic aperture radar systems operating at around 100 GHz have indicated that the use of fully polarimetric systems can lead to improvement in the image quality.[67,68] Previous investigations into terahertz imaging as an NDT technique indicate that this method has the potential to detect some fiberglass defects. Those examinations included several terahertz imaging methods such as time-domain spectroscopy and frequency-modulated continuous wave systems.[61-66] Additionally, preliminary investigations into terahertz ISAR have also shown that there are added benefits as this technique is coupled with a fully polarimetric system.[67,68] Alternatively, 5 parameters can be used (ie, Euler parameters) to estimate the maximum scattering intensity and identify the defect. [69-71]

Other researchers proposed the use of X-ray imaging for scanning the subsurface of composite material panels and detecting defects using X-ray scans on GFRP components. X-ray imaging is a technique for imaging the interior structure of objects. It relies on the different levels of absorption of X-ray photons as they pass through the material for impressing onto a photosensitive panel. While X-ray systems are most well known for medical and security screening applications, there has been an effort to apply them to nondestructive inspection of composite materials.[72] This technique has been proven to be capable of detecting damages having a diameter as small as 19×10^{-3} m on the main spar, 15×10^{-3} m on the trailing edge, and structural defects such as a lack of adhesive and internal irregularities.[73] Moreover, in recent years, portable systems have been developed using gamma rays and neutrons for detecting small cylindrical defects having subcentimeter dimensions.[74] The X-ray measurement allows for obtaining quantitative information about variations in density in the targeted object, which can indicate changes in material properties or internal delaminations. For this reason, X-ray computed tomography (CT) has proven to be a promising technique for probing the interior structure[75] and detecting various defects in glass fiber composite materials. The primary downside to CT scans is the long scan times and equipment cost. Also, the health hazards associated with X-ray operation should be considered. Preliminary investigations have indicated that simple X-ray transmission measurements can even detect subsurface defects with excellent accuracy.[67] Nevertheless, the main

drawback of this technique for being consistently used as inspection method for performing a large-scale investigation of manufacturing defects in WT blades is the cost, which can be estimated to be as high as $2 million for a utility-scale size blade inspection system. For a complete survey of these systems, interested readers may consult.[76-80]

Although there are several other methods that meet the proposed criteria of wind turbine blade assessment currently available, the authors decided to focus on imagining methods for 2 specific reasons. The first one is that the chosen methods allow the possibility to investigate subsurface defects and deterioration inside the structure that cannot be observed with other traditionally used techniques. The main reason though is the possibility of advancing the use of a method that allows visualizing the presence of a defect in a clear and intuitive manner, that do not require any specific training or advanced analysis skills, so that people working on wind turbine blade postmanufacturing control can assess the quality of the blade easily. Current trends in research are also proving that vision-based and optical sensors are techniques having higher potential to become preferred inspection methods for NDE of large-sized structures.[81]

3 | FIBERGLASS SAMPLES

The fiberglass samples included in this study were designed and fabricated by the Composites Engineering Research Laboratory (CERL) in Brunswick, ME. While the fiberglass material varied for each sample, all 4 panels were created using Hexion RIMR 135 epoxy resin and Hexion RIMH 1366 amine hardener mixed at a ratio of 100:30 respectively. Dimensions of each sample are roughly 0.45 × 0.75 × 0.03 m. Four panels have been fabricated, each having a set of specific embedded defects emulating those that are typically found in WT blades' spar caps as a result of the manufacturing process. It should be pointed out that while a full-scale blade's structure is more complicated than these simple panels (ie, thickness and shape variation), complicating the geometry of preliminary investigation is not necessary at this stage. In this paper, to obtain a baseline understanding of the 3 abovementioned NDT methods' performance, panels similar in scale and scope to those used in research performed at Sandia National Laboratory were fabricated and used.[60] It is common to test NDT techniques on controlled samples where the size and severity of defects are known before applying techniques to full-scale blades. Additionally, for a utility-scale wind turbine blade (ie, 60+ m long), the tapered effects has an angle of nearly 13° for the first 15 m of length from the root and then it decreases gradually to zero.[82] Therefore, the full-scale blades are so large that most of their surface area can be considered with good approximation flat when considering a few square meters at a time. Adapting the final techniques to curve surfaces would simply be a matter of taking into account the various angles of incidence involved. In operational practice, systems can be designed to ensure that the device is always oriented perpendicular to the surface of the blade, and to reduce the size of the investigated field of view if areas characterized by larger curvatures are considered. Nonetheless, the present paper aims to compare 3 different techniques only and further analyses to optimize the capabilities of the best-performing technique need to be the object of further studies.

In particular, Sample_1 is a baseline panel fabricated by CERL in collaboration with TPI composites. This sample consists of 20 plies of ELT-5500 fiberglass sheets and has no intentionally embedded manufacturing defects. Sample_2 consists of 20 plies of ELT-5500 fiberglass sheets with several out-of-plane wave defects of various types integrated at the 10th layer. Three different techniques for inducing the artificial wave defects were used. Those included resin rod inserts, an s-fold defect, and a glass pyramid insert as summarized in Table 1. The third panel,

TABLE 1 Descriptions and geometrical characteristics of defects embedded in fiberglass Sample_2, Sample_3, and Sample_4

Sample_2		Sample_3		Sample_4	
Defect Number (Ref. Figure 3B)	**Defect Type and Size**	**Defect Number (Ref. Figure 3C)**	**Defect Type and Size**	**Defect Number (Ref. Figure 3D)**	**Defect Type and Size**
1	12.7×10^{-3} m (0.50″) cured semicylinder resin rod insert	1	Silicone strip insert	1	Crimping iron-induced wave defect (least severe)
2	5.1×10^{-3} m (0.20″) cured semicylinder resin rod insert	2	No contaminant, true de-wet	2	Wave defect induced using 6.3×10^{-3} m (1/4″) dowel
3	2.5×10^{-3} m (0.10″) cured semicylinder resin rod insert	3	50.8×10^{-3} m (2.00″) diameter silicone dot insert	3	Wave defect induced using 9.5×10^{-3} m (3/8″) dowel
4	25.4×10^{-3} m (1.00″) s-fold in the 11th ply	4	38.1×10^{-3} m (1.50″) diameter silicone dot insert	4	s-fold defect (most severe, local ply thickness approximately tripled)
5	Glass pyramid formed by 4 layers of glass	5	31.7×10^{-3} m (1.25″) diameter silicone dot insert	5	Thickness taper (less 1 layer every 31.7×10^{-3} m (1.25″) from 20 to 16 layers)
		6	19.1×10^{-3} m (0.75″) diameter silicone dot insert	n/a	Large rectangular porosity defect

All defects are embedded 10 plies into the laminate

designated as Sample_3, consists of 20 plies of UD1800 fiberglass and contains 2 types of porosity defects. The first one includes a set of increasing diameter silicon inserts of thickness 1 mm, and a true de-wet with no material contaminant as summarized in Table 1. The fourth panel, Sample_4, is made up of 20 plies of Vectorply ELT-5500 fiberglass sheets. This sample contains 4 intentionally embedded out-of-plane fiber wave defects integrated 10 plies into the laminate. The flaws increase in severity from the left side of the defect schematic shown in Figure 3D to the right-hand side. In addition, there is a thickness taper in the sample where the thickness changes in steps from 20 plies to 16 plies thick on the rightmost edge of the specimen. Each thickness step is 1 in wide. Sample_4 also contains a significant oval-shaped porosity defect in the center of the sample, which is visible in the photograph of the front of the object shown in Figure 3D. This defect is a result of trapped air that was caused while the resin was being infused into the dry fiber. This defect is not shown in the defect schematic, as it was not intentionally embedded into the sample. Pictures of the different panels are shown in Figure 3 in comparison to a metal bar 3.05×10^{-1} m long (1 ft). The figure also shows a schematic description of the embedded defects and a detailed view of the most significant ones.

As can be observed from pictures shown in Figure 3, each characteristic of the panels is representative of a typical defect which can occur during the manufacturing process of a WT blade. In particular, wave defects simulate the nonparallel alignment of the fabric layers that are induced during the VARTM process. The silicon inserts replicate possible inclusions, while the true de-wet defect emulates the presence of potential resin dry areas. Finally, the thickness taper region mimics ply drops in the composite layup. Note that defects 4 and 5 in Sample_2, defect 1 in Sample_3, and defects 1 to 3 in Sample_4 are not shown in the detailed view of the specimens as their dimensions cannot be appreciated in the figure.

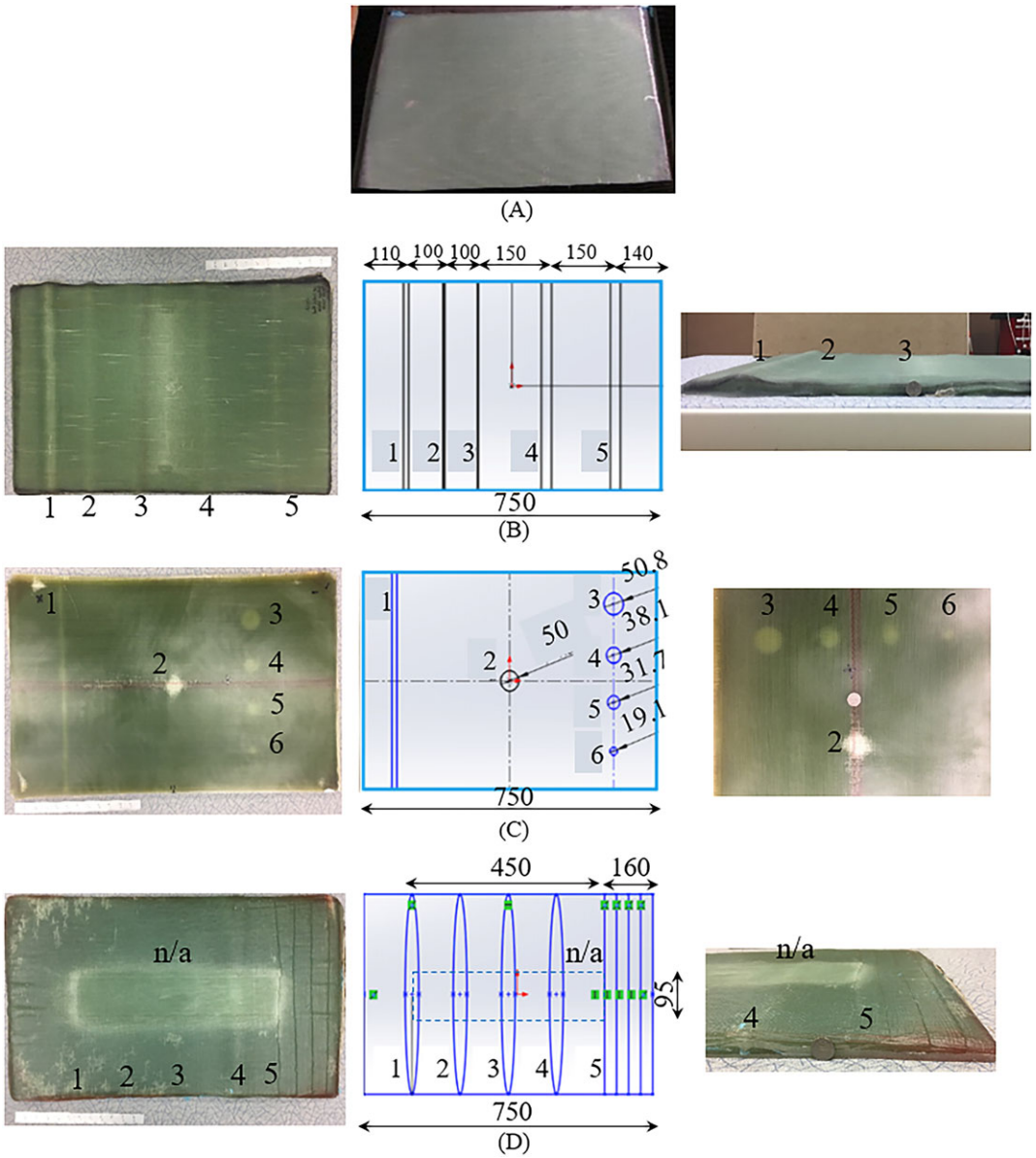

FIGURE 3 Photograph of fiberglass samples (left), schematic of defects embedded at the 10th plies (center), and detail of the defects compared to a US quarter dollar coin (right). A, Sample_1 baseline sample with no artificially induced defects. B, Sample_2 with out-of-plane wave defects. C, Sample_3 with silicon inserts and true de-wet defects. D, Sample_4 with out-of-plane fiber wave defects and thickness taper region. Dimensions in mm [Colour figure can be viewed at wileyonlinelibrary.com]

4 | EVALUATION OF THE SELECTED NDT TECHNIQUES PERFORMANCE

Terahertz ISAR, IRT, and X-ray imaging are 3 noncontact, full-field measurement techniques that can be used for assessing the condition of WT blades and highlight the presence of defects in the manufacturing process. Several laboratory tests were performed to (i) investigate the accuracy of the systems in identifying the presence of defects and (ii) compare the results obtained from a common set of test samples to evaluate the potential of each system.

4.1 | Terahertz inverse synthetic aperture radar

The terahertz scattering data were collected using a 100 GHz compact radar range. The system illuminates the target sample with terahertz radiation, stepping through a band of frequencies of at least 16 GHz. The system measured the magnitude and phase of the radiation reflected back toward the receiver, which has a fixed bistatic angle of 0.3° to the transmitter.

The system then rotates the target sample and repeats the measurement to collect data through a full range of angles in azimuth. A diagram for this setup is shown in Figure 4.[83] The sample rotation is used to create a synthetic aperture, and images are generated from the scattering data using inverse synthetic radar (ISAR) techniques. A 2-dimensional Fourier transform of this scattering data transforms the data, which was initially a function of frequency and azimuthal angle, into data that is a function of range and crossrange. By combining multiple ISAR images, each generated at different angles in azimuth, into a single composite image produces a notable increase in the visibility of defects within the images. [67]

The images shown in Figure 5 were generated by taking several ISAR images created at different azimuthal angles and backrotating them to the 0° azimuth position. The scattering values for each pixel are then averaged to produce a grid of averaged scattering values for each pixel. The 4 fiberglass samples described in Section 3 were imaged using the techniques explained above. The composite *m* parameter ISAR images for the 4 panels were generated using 360 single azimuth ISAR images at 30° elevation are shown in Figure 5 together with the schematic of the embedded defects for a more straightforward comparison. It should be noticed that in addition to the scattering from the samples themselves, scattering from specific features of the mounting apparatus are also visible in the ISAR images shown in Figure 5A. The location of the test object in each image has been outlined with a brown dashed box to help differentiate them from the mounting apparatus. The data are reported using the unit of decibel square meters (dBsm) which is relative to the scattering intensity of a metallic sphere of unit cross section.[67] The range of the color scale in Figure 5B to D has also varied to make the contrast in the images clearer. Figure 4A reveals that the ISAR image of the baseline sample is uniform to within a few dB. In Figure 5B, only the 25.4×10^{-3} m s-fold defect (the black line on the specimen in the photograph and defect #4 in the schematic) shows up clearly in the ISAR image, while it is difficult to determine the presence of any other wave defect conclusively. An accurate observation of the same picture could reveal that the terahertz system can highlight the existence of the more prominent flaw as well (ie, 12.7×10^{-3} m resin rod insert, referred to as defect 1), but its visualization is not straightforward as the 25.4×10^{-3} m s-fold defect. For results shown in Figure 5C, the ISAR image can reveal the presence of the true de-wet defect only. The silicon material inserts did not appear in this 30° elevation image, nor in any other ISAR images generated for this sample. While analyzing data obtained from the last specimen, it is possible to observe that the significant porosity defect dominates the picture, and neither the wave defects nor the thickness taper are conclusively visible in the images.

In summary, the terahertz ISAR technique has been shown to make some significant fiber wave defects and near-surface porosity defects visible, although it struggles to reveal the existence of more profound defects. It is likely explained by a lack of penetration of the 100 GHz radiation into the fiberglass samples. A lower frequency system would be recommended for further investigations of this kind of radar technique.

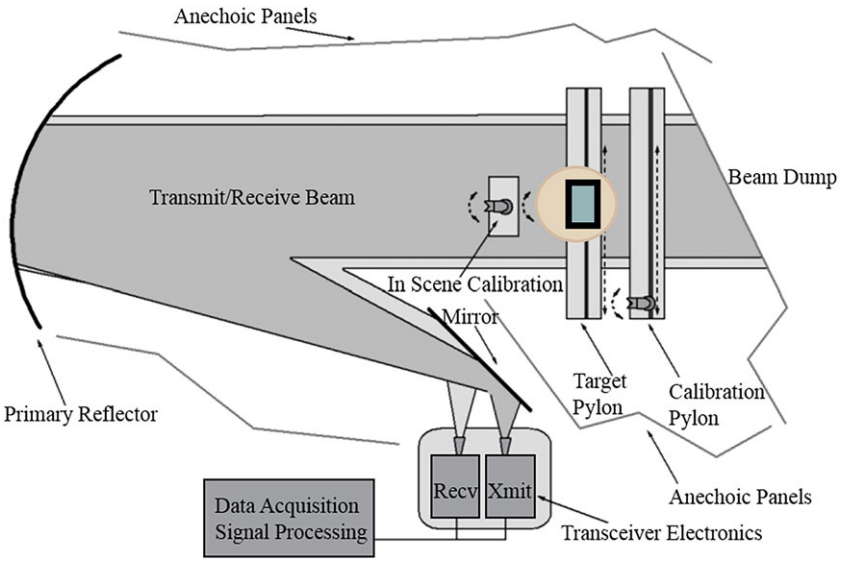

FIGURE 4 Diagram of the 100 GHz compact radar range used to collect scattering measurements. The system collects fully polarimetric scattering data across a bandwidth greater than 16 GHz[83] [Colour figure can be viewed at wileyonlinelibrary.com]

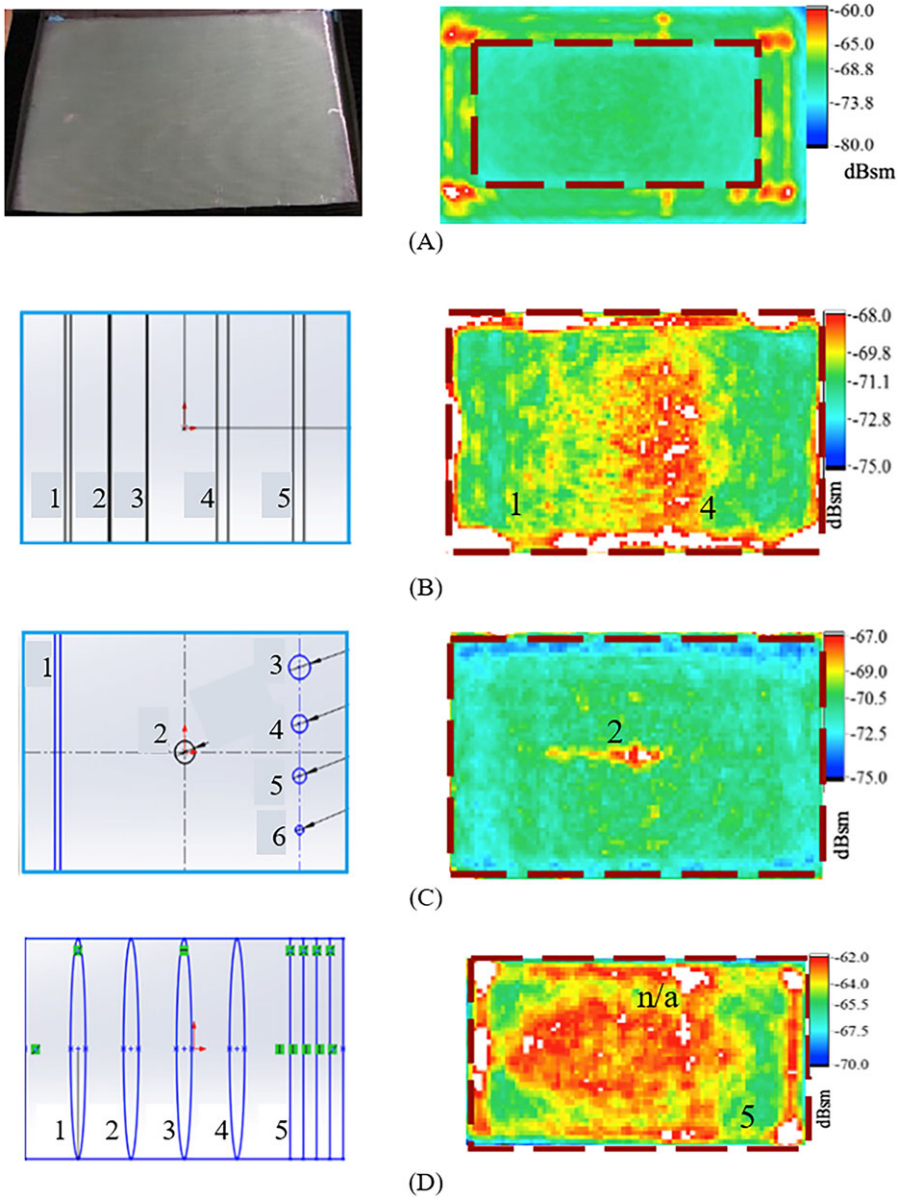

FIGURE 5 Composite *m* parameter ISAR images generated for the 3 panels analyzed (right) with the highlighted defects that can be identified and schematic of defects embedded at the 10th plies (left). A, Sample_1 baseline with no intentionally embedded defects. B, Sample_2 with out-of-plane wave defects. C, Sample_3 with silicon inserts and the true de-wet defect. D, Sample_4 with out-of-plane fiber wave defects and thickness taper region. Dimensions in mm [Colour figure can be viewed at wileyonlinelibrary.com]

Additionally, it is worth noting that the ISAR system used in this study was not designed for NDT applications. A system designed specifically with NDT in mind could improve imaging performance.

4.2 | Infrared thermography

The second set of tests aimed to evaluate the feasibility of detecting defects embedded in the panels used IRT analyses. For doing this, a PCE-TC3 multipurpose IR thermal imager manufactured by PCE Instruments was used. This portable camera has a 20° × 15° field of view (FOV), a 160 × 120 pixel resolution, and it is sensitive to temperatures between −20°C and 350°C and to long-infrared radiation having wavelength λ in the range of 8 to 14 × 10^{-6} m. To evaluate the IRT sensing, several tests were conducted on the 4 samples. The experiments consisted of warming up a surface of the panel and then measuring the emitted energy on the other surface in a setup similar to that shown in Figure 6.

As observed from Figure 6, to include the whole panel surface in the camera's FOV, the IR camera and the test panel were placed approximately 2.5 m away from each other. Moreover, the object being tested was installed within a box made of thermal insulation material (ie, 5 × 10^{-2} m thick polystyrene foam board, with a thermal conductivity *h* equal to 0.025 Wm^{-1} K^{-1}). The box contained an electrical heater used for increasing the air temperature within the enclosure, uniformly warming up the inner surface of the panel, and creating a temperature difference between the inner and outer surfaces of the specimen and to produce a thermal flux. Because of the lower thermal resistivity of the fiberglass

FIGURE 6 Thermal imaging test setup [Colour figure can be viewed at wileyonlinelibrary.com]

panel compared to the foam board, the heat flux can be considered to be coming out from only the fiberglass panel. Furthermore, a thermometer was used for controlling the temperature inside the enclosure, while a thermocouple was used for measuring the temperature of the external surface of the panel and correcting the temperature recorded by the camera. This operation was necessary because the emissivity of the panel is not known. For this reason, the values recorded using the thermal imager have to be modified taking into account the exact temperature values recorded at well-known positions.

Figures 7–10 present the thermal profiles measured in false colors superimposed on an image of the investigated panels and the first and second-time derivatives of temperature calculated for each of the tests performed. In particular, the thermal images shown in these examples refer to time in which the thermal flux radiated through the panels has reached the steady state (eg, 4 hours from the beginning of the test).

As observed from Figure 7, the presence of wave defects in Sample_2 can be detected. Thinner areas are characterized by higher values of temperature (ie, 41.8°C), if compared to those characterized by the presence of the defects and then by the bigger thickness (ie, 41.1°C). Four of the embedded wave defects can be easily recognized, while one of those in the lower part of the panel (ie, defect designated with a 2 in Figure 3B) is confused with the noise produced in the image by the heating system. A better understanding of the defects' position in the lower part of the panel can be obtained analyzing the first time derivative of temperature in Figure 8. A general idea of the location of the defect can be identified, but the quality of the image is not as clear for the other flaws. For this purpose, a different and more uniform heating system (eg, ventilation) should be used for obtaining more accurate results. On the other hand, when the silicon embedded panel and the true de-wet defect is considered, no information can be obtained from the thermal analysis of the sample. As observed from Figure 9, none of the porosity defects embedded in the panel can be detected. The specimen has a homogeneous temperature profile, and no temperature changes are observed locally to highlight the presence of defects. The same consideration can be drawn from the analysis of the first and second-time derivatives of temperature shown in Figure 10.

One of the possible explanation for this behavior can be found in the difference of the overall heat transfer coefficient U (also called thermal transmittance) of the diverse sections of the panel. Regarding a whole part of the fiberglass panel having a thickness of 25×10^{-3} m and a value of the thermal conductivity h equal to 0.05 $Wm^{-1}\ K^{-1}$, the overall heat transfer coefficient of the section will be equal to 1.504 $Wm^{-2}\ K^{-1}$. When a section of the panel characterized by the presence of a wave defect is considered, the thickness of that section increases up to 28×10^{-3} m. It leads to a decrease in the value of the overall heat transfer coefficient of nearly 8% (U = 1.426 $Wm^{-2}\ K^{-1}$), which produces a sensible change in the transmitted heat and the temperature measured on the panel's outer face. On the contrary, when a 1×10^{-3} m thick layer of silicone (having a thermal conductivity h equal to 0.2 $Wm^{-1}\ K^{-1}$) is embedded in the fiberglass matrix, the resulting overall heat transfer coefficient U is reduced by 0.75% (U = 1.493 $Wm^{-2}\ K^{-1}$). This variation is too small for producing changes in the transmitted energy detectable with the thermal camera. The IRT analysis cannot identify any of the embedded defects. The technique has 2 primary limitations: The method is limited to defects at least 2×10^{-3} m thick, and by differences in the thermal properties between healthy and defective regions. Use of an IR camera with better thermal resolution could help overcome these issues.

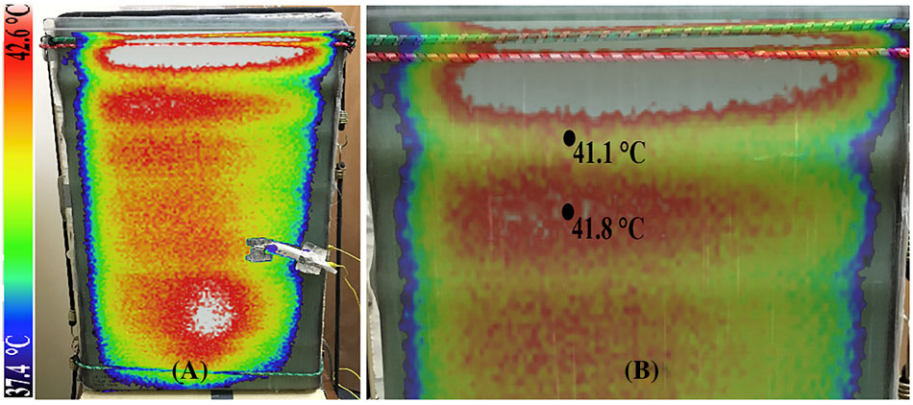

FIGURE 7 IRT recorded during the heating process of Sample_2 containing embedded out-of-plane wave defects. A, Temperature map superimposed to the test object. B, Detail of the recorded images with temperature measured in correspondence of a defect (26.5×10^{-3} m thick section) and in correspondence of a healthy area (25.4×10^{-3} m thick section) [Colour figure can be viewed at wileyonlinelibrary.com]

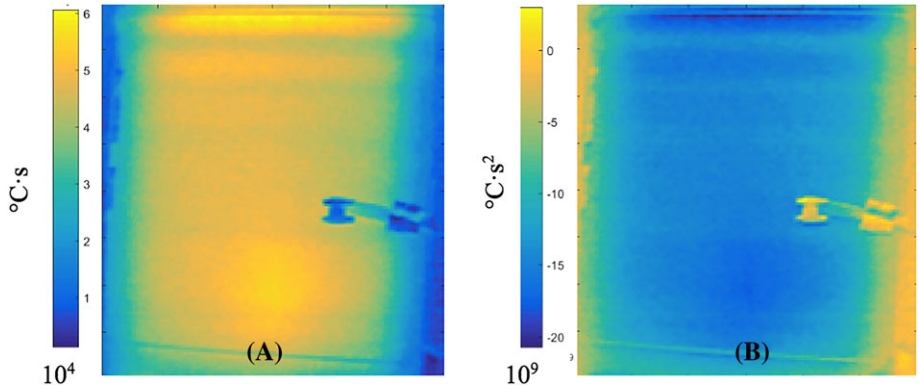

FIGURE 8 Postprocessed data from IRT analysis for Sample_2 containing embedded out-of-plane wave defects. A, First-time derivative of temperature. B, Second-time derivative of temperature [Colour figure can be viewed at wileyonlinelibrary.com]

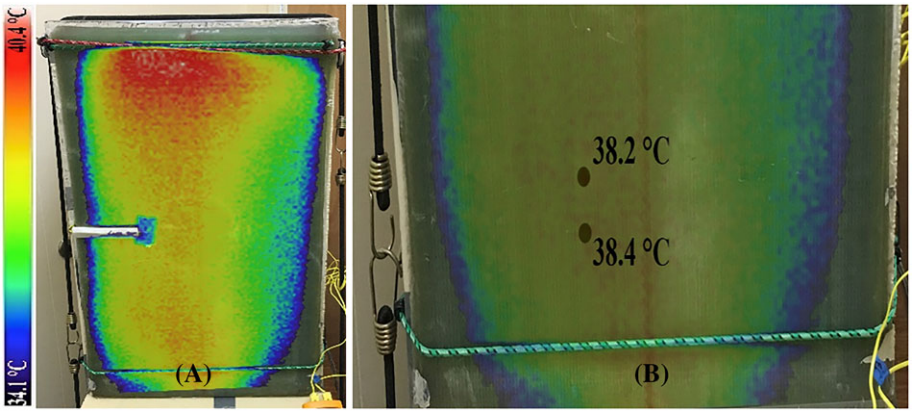

FIGURE 9 IRT recorded during the heating process of Sample_3 containing silicon inserts and the true de-wet defect. A, Temperature map superimposed to the test object. B, Detail of the recorded images with temperature measured in correspondence of a defect (1×10^{-3} m thick silicon insert) and in correspondence of a healthy area (fiberglass only, 25.4×10^{-3} m thick section) [Colour figure can be viewed at wileyonlinelibrary.com]

The results of the tests performed on Sample_4 are shown in Figure 11. In particular, the image shows the full-field IRT recorded on the surface of the panel and the temperature at specific points characterized by the presence of defects, the temperature profile through a longitudinal section of the object being tested, and a schematic of the defects embedded in the sample examined. As observed from Figure 11, the presence of thickness taper regions is identified as IRT is used. Even if not very visible, at least 3 strips characterized by slight changes in the tone of the red shadow plotted in the leftmost part of Figure 11 can be observed. Because of the low resolution of the IR camera used, and the small changes in the panel local thickness in that area, imaging of these defects is not very clear, but they can be detected. The IRT tests can identify at least 1 of

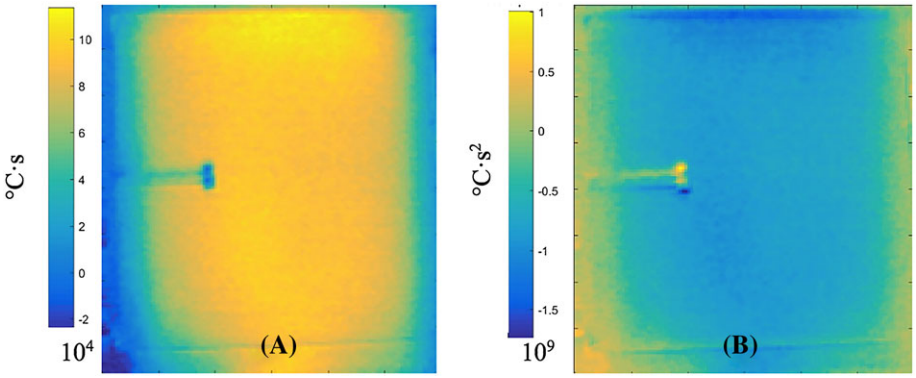

FIGURE 10 Postprocessed data from IRT analysis for Sample_3 containing embedded silicon inserts and the true de-wet defect. A, First-time derivative of temperature. B, Second-time derivative of temperature [Colour figure can be viewed at wileyonlinelibrary.com]

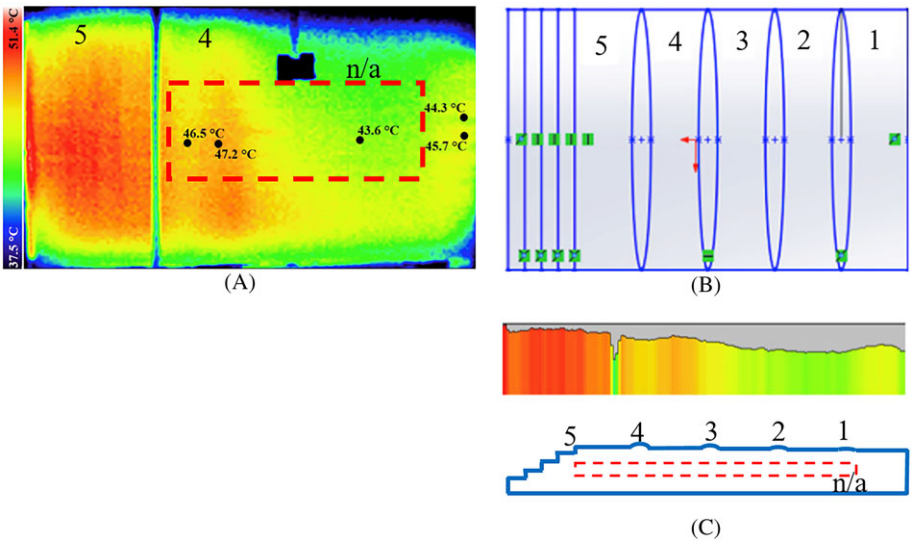

FIGURE 11 Results of the IRT tests performed on Sample_4 containing out-of-plane fiber wave defects and thickness taper region. A, IRT recorded during the heating process with temperature measured in correspondence of different areas with the highlighted defects that can be identified. B, Schematic of defects embedded in Sample_4. C, Temperature profile and longitudinal section of the sample. Dimensions in mm [Colour figure can be viewed at wileyonlinelibrary.com]

the out-of-plane fiber wave defects. Indeed, as observed in Figure 11A, the temperature of the panel changes locally in correspondence of the leftmost wave from 46.5°C to 47.2°C. Because of the increase in thickness caused by the presence of the defect, the temperature recorded on the surface was lower when compared to the healthy and thinner areas.

The thermal imaging makes it possible to detect the presence of the large oval-shaped porosity defect caused by trapped air in the middle of the sample (ie, the light green rectangle visible in the left part of Figure 3D indicated as defect n/a). Because air is an excellent thermal insulator, the presence of this defect results in a decrease of the surface temperature of the panel. As observed in Figure 11B, the temperature profile drops in correspondence of this flaw from 45.7°C to 43.6°C. The presence of the porosity defect masks the other 3 out-of-plane fiber wave defects embedded in Sample_4. The IRT technique highlights some other flaws like the 4 small waves visible in the left edge of the image plotted in Figure 3D, characterized by local changes in temperature (ie, 45.7°C for the healthy area and 44.3°C in correspondence with the wave defects).

4.3 | X-ray imaging

The fiberglass samples were also imaged in a PX 10.10 MV nonpalletized freight X-ray system developed by L3 Technologies, similar to that shown in Figure 12.[84]

This system has a 160 kV X-ray source located underneath a conveyor belt and an array of detectors at the top of the system. During the test, each of the samples was placed on the inspection surface (flat side) face down on the conveyor belt. The images recorded using the X-ray scanner mentioned above scanner for the 4 panels; Sample_2, Sample_3, and Sample_4 are shown in Figure 13 together with the schematic of the embedded defects for a more straightforward comparison.

FIGURE 12 Photograph of the PX 10.10 MV nonpalletized freight X-ray model system[84] [Colour figure can be viewed at wileyonlinelibrary.com]

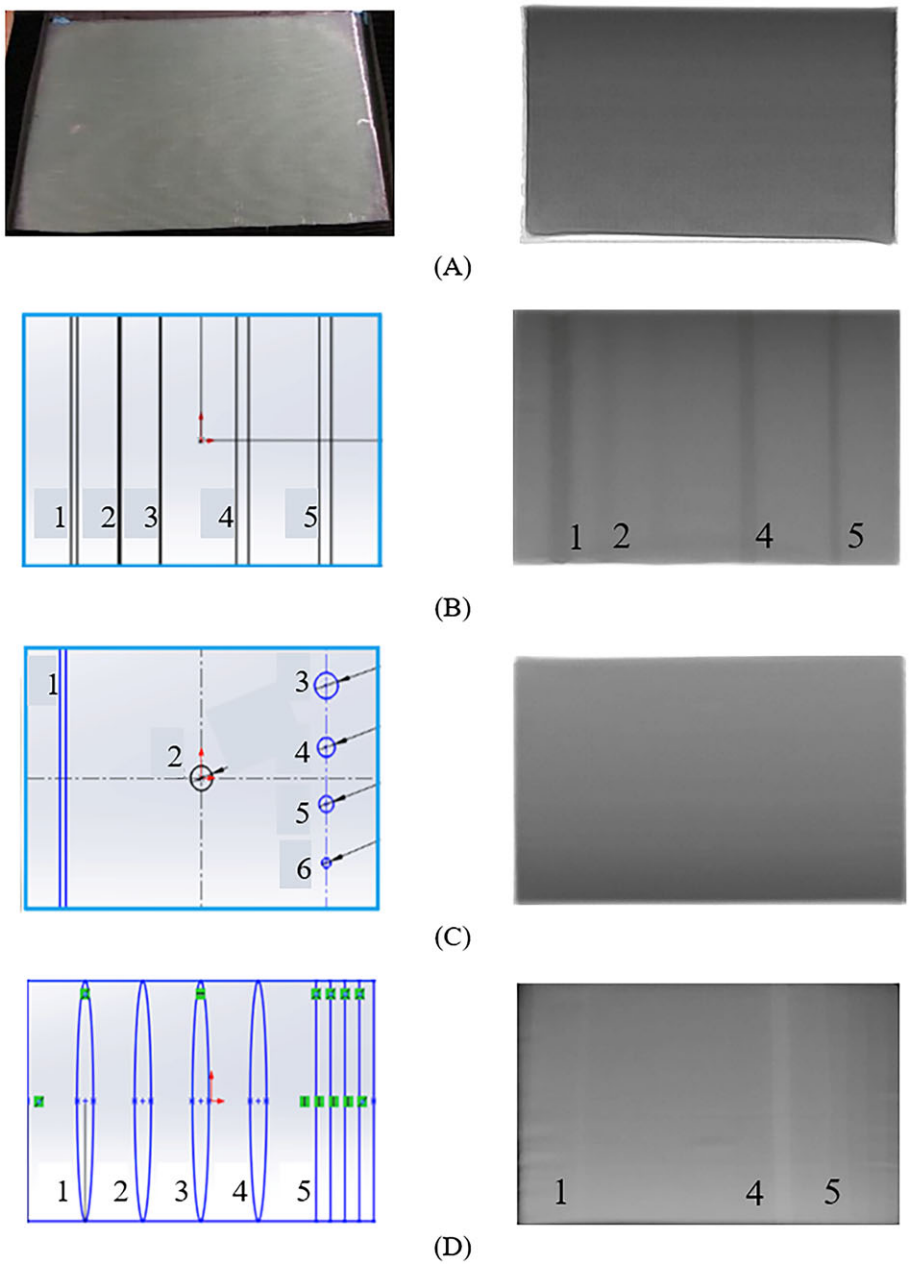

FIGURE 13 X-ray imaging generated for the 3 panels analyzed (right) with the highlighted defects that can be identified and schematic of defects embedded at the 10th plies (left). A, Sample_1 baseline with no intentionally embedded defects. B, Sample_2 with out-of-plane wave defects. C, Sample_3 with silicon inserts and the true de-wet defect. D, Sample_4 with out-of-plane fiber wave defects and thickness taper region [Colour figure can be viewed at wileyonlinelibrary.com]

Figure 13B shows that it is possible to observe that the larger wave defects (ie, those indicated with 1, 4, and 5) are visible in the image. The smaller wave defects (ie, 2 and 3) are also apparent, but the contrast is not as noticeable. The X-ray scanning system is very effective at detecting wave defects. Similar to what observed for the other 2 techniques, the X-ray imaging is not useful in identifying any of the flaws characterizing Sample_3. In particular, neither the silicone inserts nor the surface true de-wet is visible in any of the X-ray images recorded. This is likely because of the silicone strips being too thin to cause any difference in the X-ray absorption properties. About Sample_4, both the leftmost (considered least severe) and the rightmost (considered most severe) wave defects are visible in the X-ray image. Also, each of the thickness taper transitions is visible in the X-ray image, indicating that this technique is highly sensitive to thickness changes in the fiberglass samples. It is worth noting that the significant porosity defect, which is strongly visible in both the photograph (Figure 3D) and the terahertz image (Figure 5D), is not visible in this X-ray image.

4.4 | Lessons learned

Any inspection system that is implemented on a wide scale must be (1) able to scan a large area quickly, (2) effective in identifying defects, and (3) relatively inexpensive, otherwise the sensing approach will not be adopted. Therefore, in this research, the team focused on technologies that met the first criterion and investigated whether the technology has the potential to satisfy the other 2. This preliminary investigation focused on relatively small, flat fiberglass samples, and one could raise the question as to whether these measurement techniques can perform effectively on full-scale, curved, wind turbine blades.

Synthetic aperture radar images of landscapes are often obtained by putting radar systems on airplanes or satellites and performing measurements during flybys.[85,86] While these applications are primarily focused on surface reflections, not penetration, they reveal SAR techniques to be robust enough to be applied to systems across a wide range of scales and surface complexities. For wind turbine blade applications in particular, SAR techniques could be implemented via a radar on gantry system that would collect radar scattering data as it moves along the length of blade. With the price of radar systems coming down because of their use in the automotive industry, SAR could potentially be implemented at low cost if its effectiveness was improved. A primary limitation of terahertz radar techniques would be the presence of the carbon fiber composite and other conducting materials inside the spar caps. Terahertz (and even millimeter wave) frequency electromagnetic radiation is unable to penetrate conducting materials, and the penetration depth of techniques utilizing this radiation is limited to the surface of the conducting material. This is true for conducting materials both on the surface of the blades and embedded in the subsurface of the target object.

Similar consideration can be drawn for the IRT method. Infrared thermography has been used for performing thermal analyses on several structures having complex geometry (eg, heritage buildings). The possibility to orient the thermal camera perpendicular to the surface being tested reduces the effect of second-reflex waves. Moreover, the use of current photogrammetric solution image orientation/sensor calibration using structure-from-motion and dense images cloud matching allows for reconstruction of accurate thermal maps of complex geometries as well.[87]

With regards to X-ray imaging, it has shown to be effective and existing systems are capable of scanning the interiors of objects having different geometries (eg, suitcases at smaller scales, trucks and shipping containers at larger scales). When placed on a gantry, an X-ray inspection system should be capable of scanning a large area of a WTB without a problem. The primary issue with a large-scale scanning X-ray system is the high cost ($1-2 M) and health safety concerns.

Table 2 summarizes the capabilities of the different technologies investigated in detecting the various manufacturing defects considered for a comparison at a glance.

The inspection times for these techniques ranged from seconds for the X-ray technique, to hours for the ISAR and IRT techniques. However, it is important to realize that some of these systems were not designed with this application in mind. The ISAR system in particular was not designed with imaging speed as a consideration, and therefore takes hours just to image a single panel. The authors are confident that a specifically designed W band radar system could achieve video rate imaging speeds. The IRT technique takes hours to image a sample because of the heating cooling cycle required for providing a difference of temperature suitable for being detected by the low-accuracy camera used in this study. The X-ray system, on the other hand, was an airport scanner designed with speed in mind, which is why it takes a matter of seconds to measure a single panel.

TABLE 2 Comparative results of the detecting capabilities of the 3 investigated NDT techniques

NDT Technique	Sample_2	Sample_3		Sample_4		
	Inclusions	Inclusions	Resin Dry Area	Out of Plane	Porosity	Thickness Taper
Terahertz ISAR	Partially	No	Yes	No	Yes	Partially
IRT	Yes	No	No	Partially	Yes	Yes
X-ray	Yes	No	No	Yes	No	Yes

5 | CONCLUSIONS

The various laboratory tests performed on the different samples have allowed evaluating the performance of the 3 techniques investigated under controlled conditions. It should be noted that this is 1 of the first research efforts done for characterizing the use of these methods together for performing NDT inspection on components of a wind turbine blade with specific reference to spare caps. For what shown so far, none of the techniques seem to provide a compressive analysis of the possible defects embedded in plies during the manufacturing process, instead of the possibility to use a particular method for a specific flaw and another system for another kind of defects. One of the primary outcomes of this research is that measurements made using all of the 3 techniques are extremely quick to be performed one the samples have been prepared. It is a well-desired feature as large surfaces have to be scanned as in the case of utility-scale WT. Terahertz ISAR systems can examine a panel within a few minutes, and the process can be automatically repeated for different azimuthal and orientation angles for a full characterization of the specimen. Infrared thermography data acquisition and processing is secure do not present an issue. The only difficulty concerns the thermal energy to be supplied to the object being tested to produce a difference of temperature (and thus emissivity) that can be measured by the sensor. A steady and slow heating of samples has shown to produce better results than flash thermography despite the longer time for providing an appreciable difference of temperature between different areas of the test object. X-ray imaging is rapid and allows scanning areas having dimensions similar to that of the samples within a few seconds.

The research also pointed out that the impossibility to detect defects depended mostly by the inherent characteristics of the sensors used in the experiments. The 100 GHz waves used for deriving the ISAR scanner does not have enough penetration power to travel through the plies and return the backscattered information. This is a primary drawback of this technique, considering that thickness of WTBs' spar caps may range from a few millimeters to a few centimeters and profound penetration power is required. For this reason, the results of this research indicate that ISAR system needs a longer wavelength to perform better. The IRT would benefit from using better resolution sensors capable of detecting smaller increment in the emissivity of a material and thus are characterized by a lower difference of temperature. Overall, both solutions would require the development of ad hoc systems with a consequent increase in the price. All methods would perform best in an indoor environment as the presence of water and moisture may affect the way electromagnetic (EM) waves are transmitted through the material, while lighting is not a problem as all the 3 system record information in regions of the EM spectrum different from the visible one.

As wind turbine blades continue to increase in size, their cost increases, and so does the need to assess their manufacturing quality to prevent defects that could jeopardize their future functionality once installed. Nondestructive testing techniques have become reliable methods for detecting the presence of defects at an early stage and to safeguard the structural stability of the blades. In this research, a great deal of attention is given to 3 different NDT techniques, and the pros and cons of their use for detecting manufacturing defects are evaluated through extensive laboratory tests. In particular, the performance of terahertz ISAR, IRT, and X-ray imaging is examined and compared to a standard set of test panels. The 3 techniques are used for performing a back-to-back comparison to detect defects embedded in the fiberglass panels that are characteristic of typical flaws that are found in composite wind turbine blades (ie, wave defects, resin dry areas, inclusions, etc.). Each of these techniques is being considered because they have the potential to scan blades over large areas to identify the presence or absence of these flaws.

The investigation into terahertz frequency radar has indicated that the technique can detect out-of-plane wave defects in several samples, but also seems to be unable to identify more profound subsurface defects with the current system. A system designed specifically for nondestructive inspection could potentially perform much better. Such a system should also operate at frequencies below 100 GHz for improved depth penetration. No problems resulted from the detection of resin dry areas because terahertz ISAR was the only one capable of identifying this kind of defect. The cost of the system, in his current configuration, is approximately 100K USD. Results provided by the investigation performed using the infrared thermography are incredibly encouraging. Infrared thermography cameras have been shown capable of detecting the presence of thickness variations in fiberglass panels (eg, thickness taper, wave, and out-of-plane defects) and areas of imperfect bonding between layers (eg, porosity). The system's primary limitation is that it is unable to detect the presence of material inclusions whose thermal properties are similar to that of the panel's resin because of the low accuracy of the system used. In its current configuration, the price of the system (ie, camera) is on the order of a few thousands of USD, while cameras costing up to 15 to 20K USD may be required for more accurate investigations. The X-ray imaging technique proved very effective at detecting defects. However, high equipment costs (up to 2 M USD for a complete system able to scan utility-scale WTB) and health safety concerns limit the technique's commercial viability for use in a wind turbine blade manufacturing setting.

The analyzed techniques have shown to be able to detect the imperfections embedded within composite materials with some grade of accuracy depending on the type of defect considered. Further developments of this research may involve the use of more accurate and well-suited devices, especially with regards to IRT and terahertz ISAR. Indeed, these 2 techniques seem to be the ones with more room for improvement for performing NDT evaluation of wind turbine blades and to perform quality assurance of the composite manufacturing process. Possible improvements may involve both the use of IR cameras capable of measuring smaller changes in the local emissivity of the targeted structure and the development of a radar system having a driving frequency that would allow a better penetration in the structure.

ACKNOWLEDGEMENTS

This material is based upon work funded by the National Science Foundation under Grant Number IIP-1362022 (Collaborative Research: I/UCRC for Wind Energy, Science, Technology, and Research). Any opinions, findings, and conclusions or recommendations expressed in this material are those

of the author(s) and do not necessarily reflect the views of the National Science Foundation. The authors would like to thank the WindSTAR Members (Aquanis Inc, EDP Renewables, Bachmann Electronic Corp, GE Energy, Huntsman, Hexion, Leeward Asset Management, LLC, Pattern Energy, and TPI Composites Inc) for the support provided during this research. The authors would also like to thank L3 Technologies for the use of their PX 10.10 MV nonpalletized freight X-ray system.

ORCID

Robert W. Martin http://orcid.org/0000-0003-3325-208X

REFERENCES

1. Global Wind Energy Council (GWEC). Global wind report. Annual market update 2015, 2016. http://www.gwec.net/wp-content/uploads/vip/GWEC-Global-Wind-2015-Report_April-2016_22_04.pdf. Accessed April 2017
2. International Energy Agency (IEA) Technology roadmap. Wind energy 2009. https://www.ieawind.org/wnd_info/IEA_Paris/Wind_Roadmap.pdf. Accessed April 2017.
3. Vachon W. Long-term O&M costs of wind turbines based on failure rates and repair costs. In: Proceedings WINDPOWER, American Wind Energy Association annual conference, Portland, OR, 2002, June: pp 2–5.
4. Schreck SJ, Robinson MC. Horizontal axis wind turbine blade aerodynamics in experiments and modeling. *IEEE Trans Energy Convers*. 2007;22(1):61-70.
5. Griffin DA, Ashwill TD. Alternative composite materials for megawatt-scale wind turbine blades: Design considerations and recommended testing. In ASME 2003 Wind Energy Symposium (pp. 191–201). American Society of Mechanical Engineers, 2003, January.
6. Veers PS, Ashwill TD, Sutherland HJ, et al. Trends in the design, manufacture and evaluation of wind turbine blades. *Wind Energy*. 2003;6(3):245-259.
7. Brøndsted P, Lilholt H, Lystrup A. Composite materials for wind power turbine blades. *Annu Rev Mat Res*. 2005;35(1):505-538.
8. Cairns D, Skramstad J, Mandell J. Evaluation of hand lay-up and resin transfer molding in composite wind turbine blade structures. In 20th 2001 ASME Wind Energy Symposium, 2001: p 24.
9. Germanischer L. Wind energy, GL wind. Possible Wind Turbine Damage, 2007. http://www.gl-group.com/industrial/glwind/3780.htm, 2007. Accessed October 2017.
10. Khan MM, Iqbal MT, Khan F. Reliability and condition monitoring of a wind turbine. In Electrical and Computer Engineering, 2005. Canadian Conference on IEEE, 2005, May, pp 1978–1981.
11. Summary of Wind Turbine Accident. http://www.caithnesswindfarms.co.uk/page4.htm. Accessed October 2017.
12. Campbell S. Annual blade failures estimated at around 3,800, WindPower Monthly, http://www.windpowermonthly.com/article/1347145/annual-blade-failures-estimated-around-3800, May 2015. Accessed October 2017.
13. Chou JS, Tu WT. Failure analysis and risk management of a collapsed large wind turbine tower. *Eng Fail Anal*. 2011;18(1):295-313.
14. Chou JS, Chiu CK, Huang IK, Chi KN. Failure analysis of wind turbine blade under critical wind loads. *Eng Fail Anal*. 2013;27:99-118.
15. Mandell JF, Ashwill TD, Wilson TJ, et al. Analysis of SNL/MSU/DOE fatigue database trends for wind turbine blade materials (No. SAND2010–7052). Sandia National Laboratories, 2010.
16. Cairns DS, Riddle T, Nelson J. Wind turbine composite blade manufacturing: The need for understanding defect origins, prevalence, implications and reliability. Contractor Report SAND2011–1004, Sandia National Laboratories, Albuquerque, NM, 2011.
17. Niezrecki C, Avitabile P, Chen J, et al. Inspection and monitoring of wind turbine blade-embedded wave defects during fatigue testing. *Struct. Health Monit*. 2014;13(6):629-643.
18. Mandell JF, Cairns DS, Samborsky DD, Morehead RB, Haugen DH. Prediction of delamination in wind turbine blade structural details. In ASME 2003 Wind Energy Symposium (pp. 202–213). American Society of Mechanical Engineers, 2003, January.
19. Sørensen BF, Jørgensen E, Debel CP, Jensen HM, Jacobsen TK, Halling K. Improved design of large wind turbine blade of fibre composites based on studies of scale effects (phase 1). Summary report, 2004.
20. McGugan M, Pereira G, Sørensen BF, Toftegaard H, Branner K. Damage tolerance and structural monitoring for wind turbine blades. *Phil Trans R Soc A*. 2015;373(2035):20140077.
21. Toft HS, Branner K, Berring P, Sørensen JD. Defect distribution and reliability assessment of wind turbine blades. *Eng Struct*. 2011;33(1):171-180.
22. Mandell JF, Samborsky DD, Cairns D. Fatigue of composite materials and substructures for wind turbine blades (No. SAND2002–0771). Sandia National Labs., Albuquerque, NM (US); Sandia National Labs., Livermore, CA (US), 2002.
23. Chakrapani SK, Dayal V, Barnard DJ, Eldal A, Krafka R. Ultrasonic Rayleigh wave inspection of waviness in wind turbine blades: Experimental and finite element method. *AIP Conf Proc*. 2012;1430(1):1911-1917.
24. Mandell JF, Samborsky DD, Wang L, Wahl NK. New fatigue data for wind turbine blade materials. In ASME 2003 Wind Energy Symposium (pp. 167–179). American Society of Mechanical Engineers, 2003, January.
25. Li S, Shi K, Yang K, Xu J. Research on the defect types judgment in wind turbine blades using ultrasonic NDT. *IOP Conf Ser Mater Sci Eng*. 2015;87(1):012056. IOP Publishing
26. Kardos JL, Duduković MP, Dave R. Void growth and resin transport during processing of thermosetting—matrix composites. In: *In Epoxy resins and composites IV*. Berlin, Heidelberg: Springer; 1986:101-123.
27. Joosse PA, Blanch MJ, Dutton AG, Kouroussis DA, Philippidis TP, Vionis PS. Acoustic emission monitoring of small wind turbine blades. *J Sol Energy Eng*. 2002;124(4):446-454.
28. Ciang CC, Lee JR, Bang HJ. Structural health monitoring for a wind turbine system: A review of damage detection methods. *Meas Sci Technol*. 2008;19(12):122001.
29. Márquez FPG, Tobias AM, Pérez JMP, Papaelias M. Condition monitoring of wind turbines: Techniques and methods. *Renew Energy*. 2012;46:169-178.

30. Lu B., Li Y., Wu X., Yang Z. A review of recent advances in wind turbine condition monitoring and fault diagnosis. In IEEE Power Electronics and Machines in Wind Applications, PEMWA, 2009: pp. 1–7.
31. Yang B, Sun D. Testing, inspecting and monitoring technologies for wind turbine blades: A survey. *Renew Sustain Energy Rev*. 2013;22:515-526.
32. Lading L, McGugan M, Sendrup P, Rheinländer J, Rusborg J. *Fundamentals for remote structural health monitoring of wind turbine blades—a preproject, Annex B: sensors and non-destructive testing methods for damage detection in wind turbine blades*. Roskilde, Denmark, Risø: Risø National Laboratory; 2002.
33. Heuer, H., Schulze, M. H., & Meyendorf, N. (2013). Non-destructive evaluation (NDE) of composites: Eddy current techniques. In *Non-Destructive Evaluation (NDE) of Polymer Matrix Composites* (pp. 33–55) Cambridge: Woodhead Publishing.
34. Matsuzaki R, Todoroki A. Wireless detection of internal delamination cracks in CFRP laminates using oscillating frequency changes. *Compos Sci Technol*. 2006;66(3–4):407-416.
35. Zhu YK, Tian GY, Lu RS, Zhang H. A review of optical NDT technologies. *Sensors*. 2011;11(8):7773-7798.
36. Steinchen W, Yang L. *Digital shearography: Theory and application of digital speckle pattern shearing interferometry*. 93 Bellingham: SPIE press; 2003.
37. Baqersad J, Poozesh P, Niezrecki C, Avitabile P. Photogrammetry and optical methods in structural dynamics—a review. *Mech Syst Signal Process*. 2017;86:17-34.
38. Di Carlo A. Thermography and the possibilities for its applications in clinical and experimental dermatology. *Clin Dermatol*. 1995;13(4):329-336.
39. Vadivambal R, Jayas DS. Applications of thermal imaging in agriculture and food industry—a review. *Food Bioproc Tech*. 2011;4(2):186-199.
40. Lega M, Kosmatka J, Ferrara C, Russo F, Napoli RMA, Persechino G. Using advanced aerial platforms and infrared thermography to track environmental contamination. *Environ Forensic*. 2012;13(4):332-338.
41. Cehlin M, Moshfegh B, Sandberg M. Visualization and measuring of air temperatures based on infrared. In 7th International Conference on Air Distribution in Rooms, 2000: pp. 339–347.
42. Chou YC, Yao L. Automatic diagnostic system of electrical equipment using infrared thermography. In Soft Computing and Pattern Recognition, 2009. SOCPAR'09. International Conference of IEEE. 2009, December, pp. 155–160.
43. Balaras CA, Argiriou AA. Infrared thermography for building diagnostics. *Energ Buildings*. 2002;34(2):171-183.
44. Kylili A, Fokaides PA, Christou P, Kalogirou SA. Infrared thermography (IRT) applications for building diagnostics: A review. *Appl Energy*. 2014;134:531-549.
45. Clark M, Gordon M, Forde MC. Issues over high-speed non-invasive monitoring of railway trackbed. *NDT & E Int*. 2004;37(2):131-139.
46. Maldague XP. Introduction to NDT by active infrared thermography. *Mater Eval*. 2002;60(9):1060-1073.
47. Bagavathiappan S, Lahiri BB, Saravanan T, Philip J, Jayakumar T. Infrared thermography for condition monitoring—a review. *Infrared Phys Technol*. 2013;60:35-55.
48. Mian A, Han X, Islam S, Newaz G. Fatigue damage detection in graphite/epoxy composites using sonic infrared imaging technique. *Compos Sci Technol*. 2004;64(5):657-666.
49. Li Y, Yang ZW, Zhu JT, Ming AB, Zhang W, Zhang JY. Investigation on the damage evolution in the impacted composite material based on active infrared thermography. *NDT & E Int*. 2016;83:114-122.
50. He RG, Kong DJ, Zeng Z, Tao N, Zhang CL, Feng LC. Bonding quality evaluation of wind turbine blades by pulsed thermography. In: International Symposium on Photoelectronic Detection and Imaging 2011: Advances in Infrared Imaging and Applications (Vol. 8193, p. 81933G). International Society for Optics and Photonics, 2011.
51. Maldague X, Marinetti S. Pulse phase infrared thermography. *J Appl Phys*. 1996;79(5):2694-2698.
52. Sfarra S, Ibarra-Castanedo C, Avdelidis NP, et al. A comparative investigation for the nondestructive testing of honeycomb structures by holographic interferometry and infrared thermography. *J Phys Conf Ser*. 2010;214(1, p. 012071). IOP Publishing
53. Szwedo M, Hellstein P. Qualitative diagnostics of wind-turbine blades inspection using active thermography. In Proceedings of the 12th International Conference on Quantitative InfraRed Thermography. Bordeaux, France, 2014.
54. Majewska K, Soman R, Mieloszyk M, Ostachowicz W. Assessment of delamination in composite beam using infrared thermography, optical sensors and terahertz technique. *Health Monit Struct Biol Syst* 10170. 2017;1017005. International Society for Optics and Photonics
55. Rumsey MA, Musial W. Application of infrared thermography nondestructive testing during wind turbine blade tests. *J Sol Energy Eng*. 2001;123(4):271-271.
56. Meinlschmidt, P., & Aderhold, J. (2006, *September*). Thermographic inspection of rotor blades. In Proceedings of the 9th European Conference on NDT.
57. Kharkovsky S, Zoughi R. Microwave and millimeter wave nondestructive testing and evaluation—overview and recent advances. *IEEE Instrum Meas Mag*. 2007;10(2):26-38.
58. Moll J, Krozer V, Arnold P, Dürr M, Zimmermann R, Salman R, ... & Scholz M. Radar-based structural health monitoring of wind turbine blades. In 19th World Conference on Non-Destructive Testing., Munich, Germany, 2016.
59. Hsu DK, Im KH, Chiou CP, Barnard DJ. An exploration of the utilities of terahertz waves for the NDE of composites. *AIP Conf Proc*. 2011;1335(1):533-540.
60. Roach D, Neidigk S, Rice T, Duvall R, Paquette J. Blade reliability collaborative: development and evaluation of nondestructive inspection methods for wind turbine blades. Sandia National Labs, Sandia Report SAND2014–16965, 2014.
61. Cristofani E, Friederich F, Wohnsiedler S, et al. Nondestructive testing potential evaluation of a terahertz frequency-modulated continuous-wave imager for composite materials inspection. *Opt Eng*. 2014;53(3):031211.
62. Vandewal M, Cristofani E, Brook A, et al.. Structural health monitoring using a scanning THz system. In Infrared, Millimeter, and Terahertz Waves (IRMMW-THz), 2013 38th International Conference on IEEE, 2013, September; pp. 1–2.
63. Ospald F, Zouaghi W, Beigang R, et al. Aeronautics composite material inspection with a terahertz time-domain spectroscopy system. *Opt Eng*. 2013;53(3):031208.

64. Friederich F, Cristofani E, Matheis C, Jonuscheit J, Beigang R, Vandewal M. Continuous wave terahertz inspection of glass fiber reinforced plastics with semi-automatic 3-D image processing for enhanced defect detection. In Microwave Symposium (IMS), 2014 IEEE MTT-S International IEEE, 2014, June, pp. 1–4.
65. Park JW, Im KH, Yang IY, et al. Terahertz radiation NDE of composite materials for wind turbine applications. *Int J Precis Eng Manuf*. 2014;15(6):1247-1254.
66. Nezadal M, Schür J, Schmidt LP. Non-destructive testing of glass fibre reinforced plastics with a full polarimetric imaging system. In Infrared, Millimeter, and Terahertz waves (IRMMW-THz), 2014 39th International Conference on IEEE pp. 1–2, 2014, September.
67. Martin R, Baird CS, Giles RH, Niezrecki C. Terahertz ISAR and x-ray imaging of wind turbine blade structures. *Smart Mater Nondestruct Eval Energy Syst*. 2016;9806:98060I. International Society for Optics and Photonics
68. Knott EF, Shaeffer JF, Tuley MT. *Radar cross section*. 2nd ed. Boston, MA: Artech House; 1993.
69. Huynen JR. Phenomenological theory of radar targets. Ph. D. Thesis. Technical University, Delft; 1970.
70. Kennaugh EM Polarization properties of radar reflections. M. Sc. Thesis, Ohio state University, Columbus, OH; 1952.
71. Baird CS Design and analysis of an Euler transformation algorithm applied to full-polarimetric ISAR imagery, PhD dissertation, University of Massachusetts Lowell. Lowell, MA; 2007.
72. Bossi RH, Cooprider KK, Georgeson GE. *X-ray computed tomography of composites*. Seattle Wa: Boeing Aerospace and Electronics Co; 1990.
73. Jasinien E, Raiutis R, Voleiis A, Vladiauskas A, Mitchard D, Amos M. NDT of wind turbine blades using adapted ultrasonic and radiographic techniques. *Insight-Non-Destr Test Cond Monit*. 2009;51(9):477-483.
74. Fantidis JG, Potolias C, Bandekas DV. Wind turbine blade nondestructive testing with a transportable radiography system. *Sci Technol Nucl Installations*. 2011;2011:1-6.
75. Shen H, Nutt S, Hull D. Direct observation and measurement of fiber architecture in short fiber-polymer composite foam through micro-CT imaging. *Compos Sci Technol*. 2004;64(13–14):2113-2120.
76. Tchakoua P, Wamkeue R, Ouhrouche M, Slaoui-Hasnaoui F, Tameghe TA, Ekemb G. Wind turbine condition monitoring: State-of-the-art review, new trends, and future challenges. *Energies*. 2014;7(4):2595-2630.
77. Rajic N. Principal component thermography for flaw contrast enhancement and flaw depth characterisation in composite structures. *Compos Struct*. 2002;58(4):521-528.
78. Yang R, He Y. Optically and non-optically excited thermography for composites: A review. *Infrared Phys Technol*. 2016;75:26-50.
79. Amenabar I, Mendikute A, López-Arraiza A, Lizaranzu M, Aurrekoetxea J. Comparison and analysis of non-destructive testing techniques suitable for delamination inspection in wind turbine blades. *Compos Part B Eng*. 2011;42(5):1298-1305.
80. Yang R, He Y, Zhang H. Progress and trends in nondestructive testing and evaluation for wind turbine composite blade. *Renew Sustain Energy Rev*. 2016;60:1225-1250.
81. Soman R, Majewska K, Mieloszyk M, Ostachowicz W. Damage assessment in composite beam using infrared thermography, optical sensors and terahertz technique. *J Nondestruct Eval Diagnostics and Prognostics of Eng Syst*. 2017;1(3):031001.
82. Lindenburg C. Aeroelastic modelling of the LMH64-5 blade. Energy Research Center of the Netherlands, Technical Report No. DOWEC-02-KL-084/0, 2002.
83. DeMartinis GB, Couloumbe MJ, Morgan TM, et al. *A 100 GHz polarimetric compact radar range for scale-model radar cross section measurements*. Lowell, MA: Massachusetts Univ Lowell Submillimeter-Wave Tech Lab; 2013.
84. L3 Technologies website. http://www.sds.l-3com.com/xray/PX-10-10-mv.htm. Accessed July 14, 2017.
85. Scaioni M, Rosina E, L'Erario A, Dìaz-Vilari o L. Integration of infrared thermography and photogrammetric surveying of built landscape. International Archives of the Photogrammetry, Remote Sensing & Spatial Information Sciences, 42, 2017.
86. Zebker HA, Goldstein RM. Topographic mapping from interferometric synthetic aperture radar observations. *J Geophys Res Solid Earth*. 1986;91(B5):4993-4999.
87. Curlander JC, McDonough RN. *Synthetic aperture radar*. 396 New York, NY, USA: John Wiley & Sons; 1991.

How to cite this article: Martin RW, Sabato A, Schoenberg A, Giles RH, Niezrecki C. Comparison of nondestructive testing techniques for the inspection of wind turbine blades' spar caps. *Wind Energy*. 2018;1–17. https://doi.org/10.1002/we.2208